



**Cite this article:** Rafsanjani A, Stiefel M, Jefimovs K, Mokso R, Derome D, Carmeliet J. 2014 Hygroscopic swelling and shrinkage of latewood cell wall micropillars reveal ultrastructural anisotropy. *J. R. Soc. Interface* **11**: 20140126.  
<http://dx.doi.org/10.1098/rsif.2014.0126>

Received: 4 February 2014

Accepted: 28 February 2014

**Subject Areas:**

biomechanics, biomaterials, biophysics

**Keywords:**

swelling and shrinkage, wood micropillar, anisotropy, latewood, cell wall, X-ray nano-tomography

**Author for correspondence:**

Ahmad Rafsanjani

e-mail: [ahmad.rafsanjani@mcgill.ca](mailto:ahmad.rafsanjani@mcgill.ca)

Electronic supplementary material is available at <http://dx.doi.org/10.1098/rsif.2014.0126> or via <http://rsif.royalsocietypublishing.org>.

# Hygroscopic swelling and shrinkage of latewood cell wall micropillars reveal ultrastructural anisotropy

Ahmad Rafsanjani<sup>1,2</sup>, Michael Stiefel<sup>1</sup>, Konstantins Jefimovs<sup>1</sup>, Rajmund Mokso<sup>3</sup>, Dominique Derome<sup>1</sup> and Jan Carmeliet<sup>1,4</sup>

<sup>1</sup>Swiss Federal Laboratories for Materials Science and Technology, EMPA, Duebendorf, Switzerland

<sup>2</sup>Department of Mechanical Engineering, McGill University, Montreal, Canada

<sup>3</sup>Paul Scherrer Institut, Swiss Light Source, Villigen, Switzerland

<sup>4</sup>ETH Zurich, Chair of Building Physics, Zurich, Switzerland

We document the hygroscopic swelling and shrinkage of the central and the thickest secondary cell wall layer of wood (named S2) in response to changes in environmental humidity using synchrotron radiation-based phase contrast X-ray tomographic nanoscopy. The S2 layer is a natural fibre-reinforced nanocomposite polymer and is strongly reactive to water. Using focused ion beam, micropillars with a cross section of few micrometres are fabricated from the S2 layer of the latewood cell walls of Norway spruce softwood. The thin neighbouring cell wall layers are removed to prevent hindering or restraining of moisture-induced deformation during swelling or shrinkage. The proposed experiment intended to get further insights into the microscopic origin of the anisotropic hygro-expansion of wood. It is found that the swelling/shrinkage strains are highly anisotropic in the transverse plane of the cell wall, larger in the normal than in the direction parallel to the cell wall's thickness. This ultrastructural anisotropy may be due to the concentric lamellation of the cellulose microfibrils as the role of the cellulose microfibril angle in the transverse swelling anisotropy is negligible. The volumetric swelling of the cell wall material is found to be substantially larger than the one of wood tissues within the growth ring and wood samples made of several growth rings. The hierarchical configuration in wood optimally increases its dimensional stability in response to a humid environment with higher scales of complexity.

## 1. Introduction

Wood, a hygromorphic material, undergoes dimensional changes in response to varying environmental humidity, i.e. it swells in wetting and shrinks upon drying [1,2]. By nature, wood has a complex hierarchical microstructure, giving rise to an anisotropic mechanical and swelling behaviour across multiple scales. The explanations for the anisotropic nature of wood swelling/shrinkage can be found at different hierarchical levels [3]. At the cellular level, *in situ* measurement of swelling and shrinkage of wood have been intensively performed by microscopic observations [4–6] and micro-computed X-ray tomography [7–10]. These investigations show that the swelling/shrinkage of earlywood tissues is anisotropic while the behaviour of latewood cells is almost isotropic. However, so far very little is known about the swelling/shrinkage properties of the wood cell walls [4,11,12] and no experimental investigation is reported on the hygroscopic swelling and shrinkage properties of the isolated wood cell wall layers. It is therefore of interest to obtain a fundamental understanding about the swelling behaviour of the wood cell wall material which seems to be the key factor in the anisotropic swelling behaviour of wood at higher levels of hierarchy.

The secondary wall of wood cells is composed of three layers, S1, S2 and S3, as shown in figure 1. The cell walls are bonded by the compound middle lamella (CML) which is composed of the primary wall and middle lamella. Each layer within the secondary cell wall can be considered as a natural fibre-reinforced

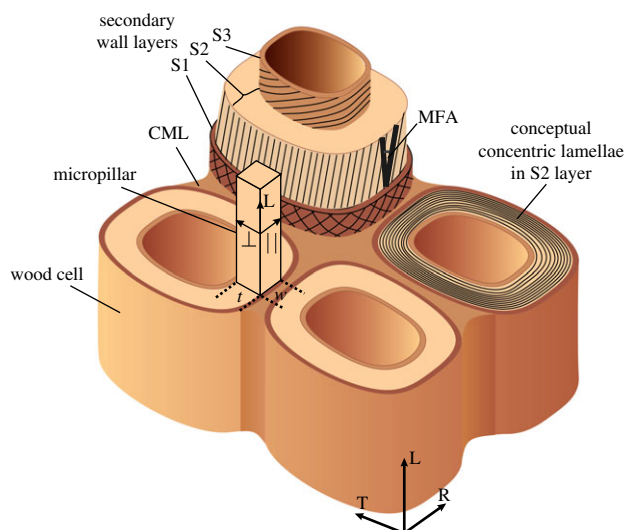


**Figure 1.** Schematic of cell wall layers within cellular structure of wood. The S2 micropillar and the local directions, normal ( $\perp$ ), parallel ( $\parallel$ ) and longitudinal (L), are indicated in this figure. The concept of concentric lamellae in S2 layer is schematically shown for one cell. (Online version in colour.)

composite where the stiff hydrophobic crystalline cellulose microfibrils are closely packed in a hydrophilic matrix of amorphous cellulose, hemicelluloses and lignin. The central and the thickest layer (named S2) is the most important structural component of the cell wall, which provides mechanical support for the tissue. The precise arrangement of the cellulose fibrils happens synchronously with cellulose synthesis. The cellulose synthase complex, also called rosette, is a transmembrane protein complex that extrudes glucose molecules and assembles them into glucan chains. Positioned in the cell membrane, the rosettes are known to be motile and believed to be attached directly or via scaffold proteins to guiding rails, the microtubules, located within the living cell [13]. It is the extruded cellulose, exiting perpendicularly to the cell membrane and then curving to lie on the cell surface, that thrusts further the synthase complex along the microtube direction [14]. Thus, the cellulose microfibrils are deposited in the limited space between the living cell and the earlier deposited rigid cell wall, in a quasi-parallel fashion with a preferential pitch to the longitudinal axis of the cell which is called microfibril angle (MFA). In the S2 layer, the cellulose microfibrils are nearly parallel to the long axis of the cell in a right-hand spiral with an MFA of about  $10^{\circ}$ – $30^{\circ}$  while, in the S1 and S3 layers, the cellulose microfibrils are nearly perpendicular to the cell axis [15]. It is generally assumed that, owing to the gradual, cumulative deposition of cellulose microfibrils which is involved in the growth of secondary cell walls, the microfibrils are configured in a concentric lamellae pattern [16], which is schematically illustrated in figure 1.

Given the large volume fraction of the S2 layer within the cell wall, we may conclude that it has also the main contribution in swelling/shrinkage behaviour. Particularly, in the transverse plane of wood, the main moisture-induced deformations occur in the S2 layer. Sorption of water molecules in the hydrophilic matrix pushes the constituents apart, resulting in formation of new pores [17] and giving rise to swelling and softening of the matrix [18]. However, the S2 material is not available for direct measurement since its microscopic dimensions make isolation by manual manipulation a challenge. Alternatively, the focused ion beam (FIB) technique allows

micro-scale samples to be prepared from individual structural components of the wood cell wall which otherwise are not accessible for testing. In recent years, the FIB has been successfully used by many researchers to prepare wood micropillars from the S2 layer for *in situ* mechanical testing in order to investigate the deformation and failure mechanism of the wood cell wall material in dry state [19–22].

In this work, we quantify the three-dimensional sorption-induced swelling and shrinkage of the S2 layer of latewood cell walls by high-resolution synchrotron radiation-based phase contrast X-ray nano-tomography (srPCXTN) which provides images with spatial resolution in the sub-100 nm range [23]. With the aid of the FIB technique, micropillars with a cross section of the size of a few micrometres are fabricated from the S2 layer of the latewood cell walls of Norway spruce softwood. The micropillars are subjected to different relative humidities and the swelling/shrinkage deformations are documented. The acquired datasets are analysed with image processing tools and the moisture-induced strains are determined. By interpreting the deformation fields derived from X-ray nano-tomography datasets in terms of the architecture of the cell wall materials, we intended to gain further insight into the role of ultrastructural configurations of the wood cell wall substance on the swelling/shrinkage anisotropy of wood at higher levels of hierarchy.

## 2. Material and methods

The wood species selected for this study was Norway spruce softwood (*Picea abies* (L.) Karst.). Wood in the living tree is formed and functions in an essentially water-saturated environment [3]. Once formed, the part of xylem active in water transport is usually at high moisture content (MC); however, the core of the trunk may have quite dried sections. In any case, in applications, wood is used in a much dryer state which varies with varying environmental conditions. Thus, this study looks at moisture variation in the hygroscopic domain, of special relevance for engineering applications. Wood is known to exhibit reversible behaviour in the 0–30% MC hygroscopic domain. The hydrophilic polymeric components of wood display similar water sorption curves, thus changes in MC seem to occur quite uniformly in these components and are totally recoverable [24,25]. The reproducibility of water sorption in wood is a strong indication of the permanence of the wood cell wall structure under drying and wetting.

For the preparation of cell wall micropillars, latewood cells were chosen since they have the largest cell wall thickness within the growth ring. Specimens of wood cubes of  $10\text{ mm}^3$  with excellent alignment of the wood cells along the sample edges were prepared. Using a microtome, the radial–tangential cross section was smoothed. Then, the latewood region of the samples were separated by a razor blade and small blocks of approximately  $500\ \mu\text{m} \times 500\ \mu\text{m} \times 10\ \text{mm}$  ( $R \times T \times L$ ) were provided for micropillar preparation.

### 2.1. Preparation of latewood cell wall micropillars

The preparation of micropillars from latewood cell wall substance was carried out by combining pico-second laser (ps-laser) ablation and Ga-FIB techniques. The laser ablation allows robust material removal down to a scale of a few tens of micrometres, while a slow but precise FIB technique allows a pillar of the required shape and dimensions to be cut from a specific cell wall region, as shown in figure 2. Using ps-laser ablation apparatus, cylindrical

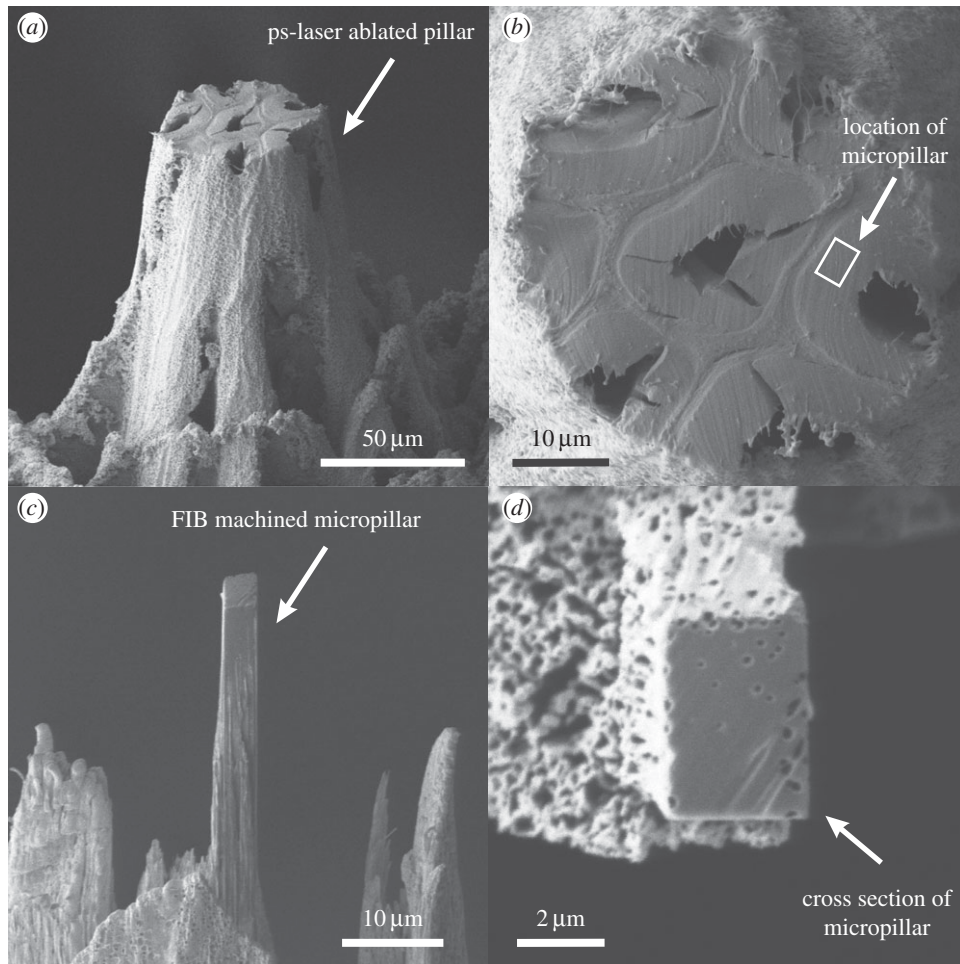


**Figure 2.** Preparation of micropillar A from latewood cell wall material by laser ablation and FIB milling. Scanning electron microscopic images of: (a) cylindrical pillar of about 50  $\mu\text{m}$  diameter is cut from a small block of latewood cells by ps-laser ablation method, (b) location of the micropillar is defined and then (c) the surrounding material is removed by rough FIB milling and (d) finally the rectangular micropillar is prepared by fine FIB machining.

pillars of approximately 50  $\mu\text{m}$  diameter and approximately 100  $\mu\text{m}$  height were machined by removing the excess material at the top of wood blocks. Each pillar contained some intact latewood cells from which one final micropillar was cut out. In the second step, for each sample, the S2 secondary cell wall layers located within a double cell wall was selected. Micropillars A and C were cut from radial walls and micropillar B was cut from the tangential wall. The sample was milled into a rectangular micropillar using a dual beam FEI Strata 235 gallium (Ga) FIB system, combined with scanning electron microscope (SEM). In order to minimize charging during SEM imaging of the wood, specimens were coated prior to FIB milling with an approximately 5 nm thick gold layer. The FIB milling was performed in three resolutions. Initially, rough milling was carried out with a high  $\text{Ga}^+$  beam current (7000 pA) to obtain a micropillar of the whole cell wall by removing its surrounding material. Next, fine polishing was performed in two steps with low  $\text{Ga}^+$  beam currents (3000 and 500 pA) to minimize beam damage and the final micropillar of the S2 secondary cell wall layer was prepared. The interaction of  $\text{Ga}^+$  ions with hemicellulose and lignin during FIB milling was seen to lead to the formation of a thin amorphous external layer which is approximately 10 nm thickness. The influence of this layer on mechanical behaviour has been found to be negligible [20]. Using this procedure, three micropillars (labelled A, B and C) were prepared. The SEM images of micropillar A at different steps of preparation are shown in figure 2. The corresponding SEM images of micropillars B and C are shown in the electronic supplementary material, figures S1 and S2. Table 1 gives the dimensions of these three micropillars and the cell wall layers from which they were fabricated.

**Table 1.** Geometrical parameters of three latewood cell wall micropillars used in this work: width  $w$  (in  $\parallel$  direction), thickness  $t$  (in  $\perp$  direction) and height  $h$  (in L direction). All dimensions are in micrometres.

micropillar	cell wall layer	$w$	$t$	$h$
A	S2	4.5	3.2	30
B	S2	5.4	2.9	22
C	S2, S1 and CML	3.8	4.6	38

As the wood cell wall is a layered composite material, there is no known structure that plays a role in joining the S1, S2 and S3 layers other than some polymeric matrix. Therefore, we expect that an isolated part of S2 keeps its mechanical integrity. However, the swelling behaviour of a micropillar grouping different layers will certainly result in a different global behaviour of S2, owing to mechanical interactions between layers.

## 2.2. Experimental procedure

The sorption-induced swelling and shrinkage of micropillars were measured by phase contrast X-ray nano-tomography. A climatic chamber was used for conditioning of the samples as explained in [7]. The chamber was an aluminium enclosure with interior dimensions of approximately 39  $\times$  15  $\times$  40 mm. The relative humidity (RH) of the chamber was controlled using an air handling and conditioning system. The bottom part was screwed to a

**Table 2.** The actual RH values measured inside the chamber in %.

set RH (%)	10	40	65	85	65	40	10
micropillar A	6	38	68	85	68	41	14
micropillar B	11	—	—	85	—	—	12
micropillar C	9	40	68	86	68	41	12

bridge that spans over the rotational stage of the tomography set-up. The top part acted as a sealed cap to enclose the space while giving access to the specimen. The chamber had two polyimide windows of  $15 \times 15$  mm, transparent to X-ray. A data acquisition system recorded the temperature and RH measured by the dew-point hygrometer and by the two relative humidity/temperature (RH/T) sensors located in the environmental chamber. Prior to measurements, the prepared micropillars were preconditioned in a desiccator with lithium chloride (LiCl) solution to keep the samples at low RH (approx. 11% RH at 25°C). Each sample was installed in the beamline for nano-tomography imaging. Using the environmental conditioning device, two micropillars, i.e. A and C, were subjected to a total six RH steps in adsorption and desorption (10 → 40 → 65 → 85 → 65 → 40 → 10% RH). Micropillar B was exposed to only one adsorption step (10 → 85% RH) and one desorption step (85 → 10% RH) owing to beam time limitation. The actual RH values measured inside the chamber are listed in table 2. At each step, the micropillars were conditioned for 45 min until equilibrium, and then tomography images were acquired.

### 2.3. Phase contrast X-ray nano-tomography

A series of synchrotron radiation-based phase contrast X-ray tomographic nanoscopy (srPCXTN) experiments [23] were conducted to document the swelling/shrinkage behaviour of micropillars at the different environmental conditions. The tomographic data were acquired at the TOMCAT beamline of the Swiss Light Source, Paul Scherrer Institut (PSI, Villigen, Switzerland). X-ray tomography ensures acquiring the full tri-dimensional information synchronously, as opposed to other methods like environmental scanning electron microscopy, laser confocal microscopy or speckle methods. Since wood has a low X-ray attenuation coefficient, the phase contrast tomography method was used. The difference in density, thus in the X-ray index of refraction is the source of phase contrast. The added advantage of using phase contrast is the very low X-ray dosage to which the sample is subjected. Scans were performed with an energy of 12 keV and 400 mA. A total number of 360 equiangular projections per tomographic scan between 0° and 180° with  $539 \times 739$  pixels was captured on a CCD camera (PCO.Edge) with a 14 bit dynamic range and an exposure time of 2 s each, resulting in a total scanning time of approximately 24 min. The dimensions of the field of view were  $32 \times 45$  μm in the horizontal and vertical directions. The effective reconstruction pixel size was about  $60 \times 60$  nm.

### 2.4. Image processing

The reconstructed tri-dimensional datasets were analysed with an intensity-based medical image registration toolbox called ELASTIX [26] with an interface to MATLAB. The micropillars were segmented based upon their greyscale values using the intermode thresholding method [27]. This method assumes a bimodal histogram and chooses the threshold to be the mean of the two peaks of the bimodal histogram. The analysed region of interest consisted of 300 slices that were grouped into three stacks of 100 slices at one pixel intervals along the longitudinal axis for micropillars A and C. Since micropillar B was

shorter, 180 slices were processed and each stack consisted of 60 slices. The swelling and shrinkage strains of micropillars between a reference state (at lowest RH approx. 10%) and each subsequent state were determined using the affine registration method as explained in detail in [7]. In brief, an affine registration is the problem of finding a linear transformation  $T(x)$  which makes a deformed volume spatially aligned to a reference volume. Mathematically, it is defined by the relation

$$T(x) = Ax + t, \quad (2.1)$$

with  $x$  the coordinates of the reference image,  $A$  a matrix referred to shear, scale and rotation contribution and  $t$  the translation vector. Under the approximation of small displacement gradients, the principal strains in three orthogonal directions at each deformed state  $i$  are given from  $\epsilon_{11}^i = A_{11} - 1$ ,  $\epsilon_{22}^i = A_{22} - 1$  and  $\epsilon_{33}^i = A_{33} - 1$ . The volumetric strains were calculated from two methods. In the first method, we initially performed a rigid registration and then we counted the number of white voxels in the segmented reference and deformed images and the volumetric strain at state  $i$  was calculated from  $\epsilon_v^i = (n_i - n_0)/n_0$ , where  $n_0$  and  $n_i$  are the number of white voxels in the reference and the deformed images, respectively. In the second approach, from the results of the affine registration, the volumetric strain was estimated as  $\epsilon_v^i = \epsilon_{11}^i + \epsilon_{22}^i + \epsilon_{33}^i$ .

The local deformation of micropillars upon swelling and shrinkage were analysed by performing a non-rigid B-spline registration between the initial reference state and each subsequent deformed state. As a result, the spatial deformation gradient field  $F$  was obtained from which the local strains were derived based on the *Eulerian* strain tensor  $\epsilon$  definition

$$\epsilon = \frac{1}{2}(\mathbf{I} - \mathbf{F}^{-T}\mathbf{F}^{-1}). \quad (2.2)$$

PARAVIEW software (Kitware, Clifton Park, NY, USA) was used for three-dimensional visualization of the tomographic datasets.

## 3. Results

The results of *in situ* quantitative assessments of hygroscopic swelling and shrinkage of FIB machined S2 micropillars by X-ray nano-tomography are presented in the following subsections. As the image resolution is bigger than the size of microfibrils, no information is available from the image on the composition inside the micropillars, the grey values being quite uniform and patterns of any sort absent. Thus, we could proceed to segment the dataset to highlight the volumes of the pillars.

### 3.1. Visualization of reconstructed nano-tomography of micropillars

Micropillars swell and shrink as the environmental condition changes. Figure 3 shows three-dimensional renderings of micropillars A, B and C at different RH states. The sorption-induced deformation of micropillars is clearly resolved in these images. The deformation occurs mainly transversally and the dimensional changes in the longitudinal direction are negligible. For micropillars A and B, the swelling is more pronounced in the direction normal to the cell wall thickness. At high RH states, the swollen micropillars exhibit a bulgy deformed shape which is not fully recovered upon the following drying steps. The swelling/shrinkage pattern is not totally uniform and some local deformation can be noticed.

In figure 4, the outlines of the three cross sections of micropillars A, B and C with a longitudinal distance of 75 slices from the top of the micropillars at dry (dashed line) and wet (solid line) states are overlaid (see unprocessed images in the

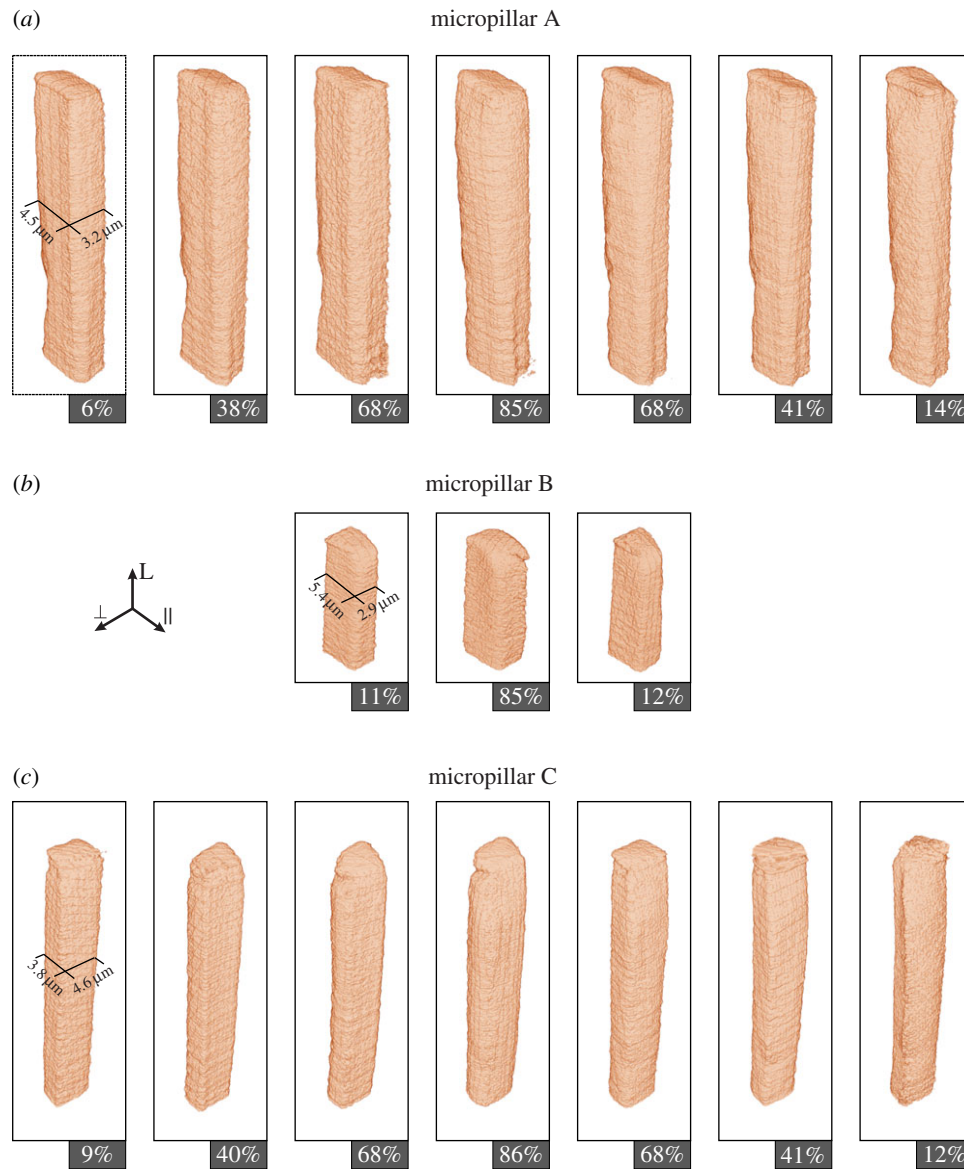


**Figure 3.** Three-dimensional visualization of latewood cell wall micropillars for different RH levels. (*a,b,c*), from left to right show the deformed state of micropillars (A, B and C) during adsorption and desorption steps. At high RH levels, swollen micropillars exhibit a bulgy deformed shape which is not fully recovered upon the following drying steps. (Online version in colour.)

electronic supplementary material, figure S3). For micropillar A, the swelling deformation in the direction perpendicular ( $\perp$ ) to the cell wall is clearly larger than the deformation in the direction parallel to the cell wall ( $\parallel$ ). Micropillar B also shows trends similar to micropillar A. The swelling of micropillar C is less anisotropic. By looking at SEM images of micropillars which are taken before FIB cutting (see the electronic supplementary material, figure S2), we can detect that micropillar C, in addition to the S2 layer, contains the S1 layer and part of CML layer. Therefore, the presence of the S1 layer with large MFA might partially restrain the swelling/shrinkage strains, thus micropillar C shows less volumetric strains. In addition, since in this configuration, a smaller volume of the cell wall swells in the perpendicular direction (i.e. S2 part), the total amount of swelling decreases.

### 3.2. Cell wall swelling/shrinkage strains determined by affine registration

Figure 5 shows the principal swelling/shrinkage strains as a function of RH for the three micropillars A, B and C obtained by affine registration. The initial state, at approximately 10%

RH, is taken as the reference and hence the strain equals zero at this state. In this figure, the strain values in directions parallel and normal to the cell wall thickness are given; the longitudinal strain values are not included as they are very small. In addition, the volumetric strains determined by affine registration, as the sum of the parallel and normal components, is compared to those obtained from voxel counting of segmented images. The results reported here are the mean value of three stacks along the height of each micropillar and the error bars show the corresponding standard deviation.

As the RH increases, we observe that micropillar A swells in the direction normal to the thickness while no significant deformation is observed in the parallel direction, i.e.  $\varepsilon_{\perp} > \varepsilon_{\parallel}$ . The amount of swelling deformation increases at high RH values. In the last adsorption step (RH: 68  $\rightarrow$  85%), the normal swelling strain increases from  $\varepsilon_{\perp} = 0.06$  to  $\varepsilon_{\perp} = 0.25$  while in the parallel direction the sample slightly shrinks and the strain is  $\varepsilon_{\parallel} \simeq 0$ . During desorption, the micropillar shrinks in both parallel and normal directions. The main shrinkage occurs in the first desorption step (RH: 85  $\rightarrow$  68%) and at the end of desorption steps when RH = 14%, the strain components in the normal and parallel directions are  $\varepsilon_{\perp} \simeq 0.08$

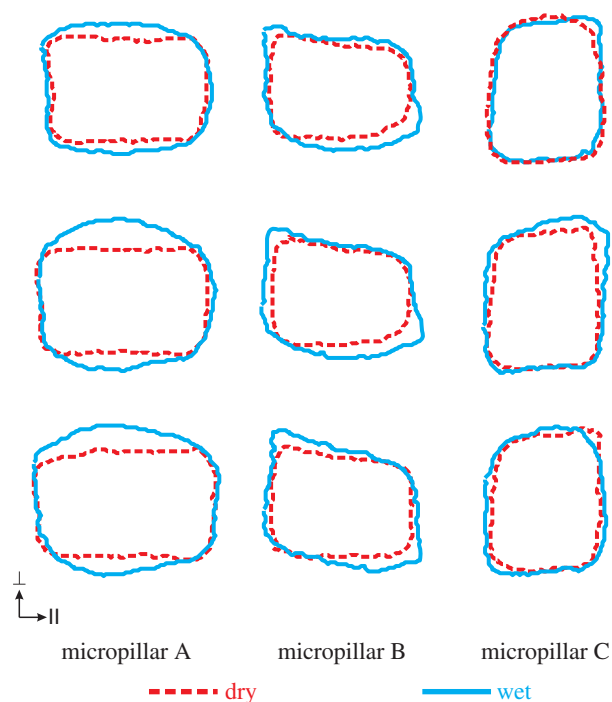


**Figure 4.** Swelling of the cross sections of the micropillars from dry to wet states. Three cross sections with a longitudinal distance of 75 slices from the top of micropillars at dry and wet states are overlaid for micropillar A (RH: 6  $\rightarrow$  85%), micropillar B (RH: 11  $\rightarrow$  85% RH) and micropillar C (RH: 9  $\rightarrow$  86%). (Online version in colour.)

and  $\varepsilon_{\parallel} \simeq -0.1$ , respectively. Both affine registration and voxel counting methods exhibit similar results for the volumetric strain. During desorption, the results are slightly different due to local deformation as will be discussed later. This agreement confirms the adequacy of the affine registration method. The swelling of micropillar A is non-reversible in this timescale. In  $\perp$  direction, the adsorption curve of the hysteresis loop is lower than the desorption one ( $\varepsilon_d > \varepsilon_a$ ) as seen at higher scale. But in  $\parallel$  direction, the situation is reversed since more deformation occurred in desorption than in adsorption ( $\varepsilon_d > \varepsilon_a$ ). Volumetrically, we see  $\varepsilon_d > \varepsilon_a$  with a quasi-reversible loop. This unusual inversion of the perpendicular and volumetric sorption curves is probably owing to the change of overall shape of the cross section, from parallelogram to elliptic. At higher RH, given the increase in moisture capacity, sorption results in large swelling strains in  $\perp$  direction as the absorbed water pushes the cell wall constituents apart, thus creating new pores. In desorption, as water molecules leave the cell wall, the newly created pores shrink and this situation may cause the buckling of the concentrically laid fibril layers. This may explain the large shrinkage of the tissue in  $\parallel$  direction.

Micropillar B was subjected to one adsorption step (RH: 11  $\rightarrow$  85%) and one desorption step (RH: 85  $\rightarrow$  12%). The swelling/shrinkage strain normal to the thickness is larger than the strain in the parallel direction; i.e.  $\varepsilon_{\perp} > \varepsilon_{\parallel}$ . This trend is similar to what has been observed for micropillar A. More specifically, at RH = 85%, the strain normal to the thickness is  $\varepsilon_{\perp} = 0.15$  which is about twofold larger than strain in the parallel direction  $\varepsilon_{\parallel} = 0.08$ . The volumetric strains obtained by affine registration and voxel counting are in excellent agreement. This measurement shows that the original configuration is fully recovered after two single adsorption and desorption steps, but as we have no information about the swelling/shrinkage behaviour at intermediate RH values, conclusions cannot be made

about the hysteresis behaviour. Furthermore, we observe that the maximum volumetric strain at RH = 85% of micropillar B is comparable to that of micropillar A. Voxel counting results are  $\varepsilon_V^A = 0.23$  and  $\varepsilon_V^B = 0.24$  while affine registration results are  $\varepsilon_V^A = 0.25$  and  $\varepsilon_V^B = 0.22$ .

Micropillar C exhibits a different swelling/shrinkage deformation pattern. During adsorption, the swelling strain is very small. In the last adsorption step (RH: 68  $\rightarrow$  86%), the sample swells in both normal and parallel directions but to a much less degree than micropillar A. The swelling strains at the end of adsorption steps in the normal and parallel directions are  $\varepsilon_{\perp} = 0.07$  and  $\varepsilon_{\parallel} = 0.11$ , respectively. As the RH decreases, it shrinks smoothly in both the normal and parallel directions. The volumetric strains obtained by both affine registration and voxel counting methods are also in accordance with a slight difference in desorption. The volume of micropillar C is almost preserved at the end of the desorption steps but the swelling/shrinkage deformation shows large hysteresis with the adsorption curve lower than the desorption. Furthermore, the maximum volumetric strain at RH = 86% is  $\varepsilon_V^C = 0.17$  which is smaller than those observed for micropillars A and B.

### 3.3. Local deformation of micropillars

The local deformations of micropillars are obtained by B-spline registration of the segmented images. The deformed state is registered to the initial dry state (approx. 10% RH) by following the surface deformation without considering the grey values inside the micropillars. Once the registration parameters are determined, the deformation field and the spatial deformation gradient field  $\mathbf{F}$  are computed. Then, the *Eulerian* strain tensor  $\varepsilon$  at each point in three dimensions can be calculated according to equation (2.2). Figure 6 shows the moisture-induced strain distribution at the surface of micropillars A, B and C in parallel ( $\parallel$ ) and normal ( $\perp$ ) directions for RH  $\simeq$  85%. Occurrence of local deformations leads to a non-uniform strain field in all micropillars. For micropillars A and B, the normal strain is larger than the parallel strain and the difference is clearly distinguishable at this high RH level. In all cases, local strain levels are in agreement with global strains obtained by affine registration method. In comparison to micropillars A and B, the strain levels of micropillar C in  $\perp$  direction are smaller.

## 4. Discussion

Owing to the hygroscopic nature of the cell wall polymers (e.g. amorphous cellulose and hemicelluloses), micropillars swell and shrink upon changes in environmental humidity. During the initial adsorption at low RH values, the rate of swelling is relatively small. This may be owing to the fact that the first water molecules sorbed find their way into interstices in the cell wall matrix and do not contribute with their full volume to the swelling of cell wall [3]. As the RH increases, the amount of swelling strain increases.

The transverse anisotropy of cell wall material is, though related, not a phenomenon identical to the swelling anisotropy of cell tissue and wood at timber scale [11]. The swelling/shrinkage coefficient is defined as the strain induced by a variation of 1% MC and is calculated from the slope of the strain curve plotted against MC. For wood, within the hygroscopic range, the moisture-induced strain is found to be a linear

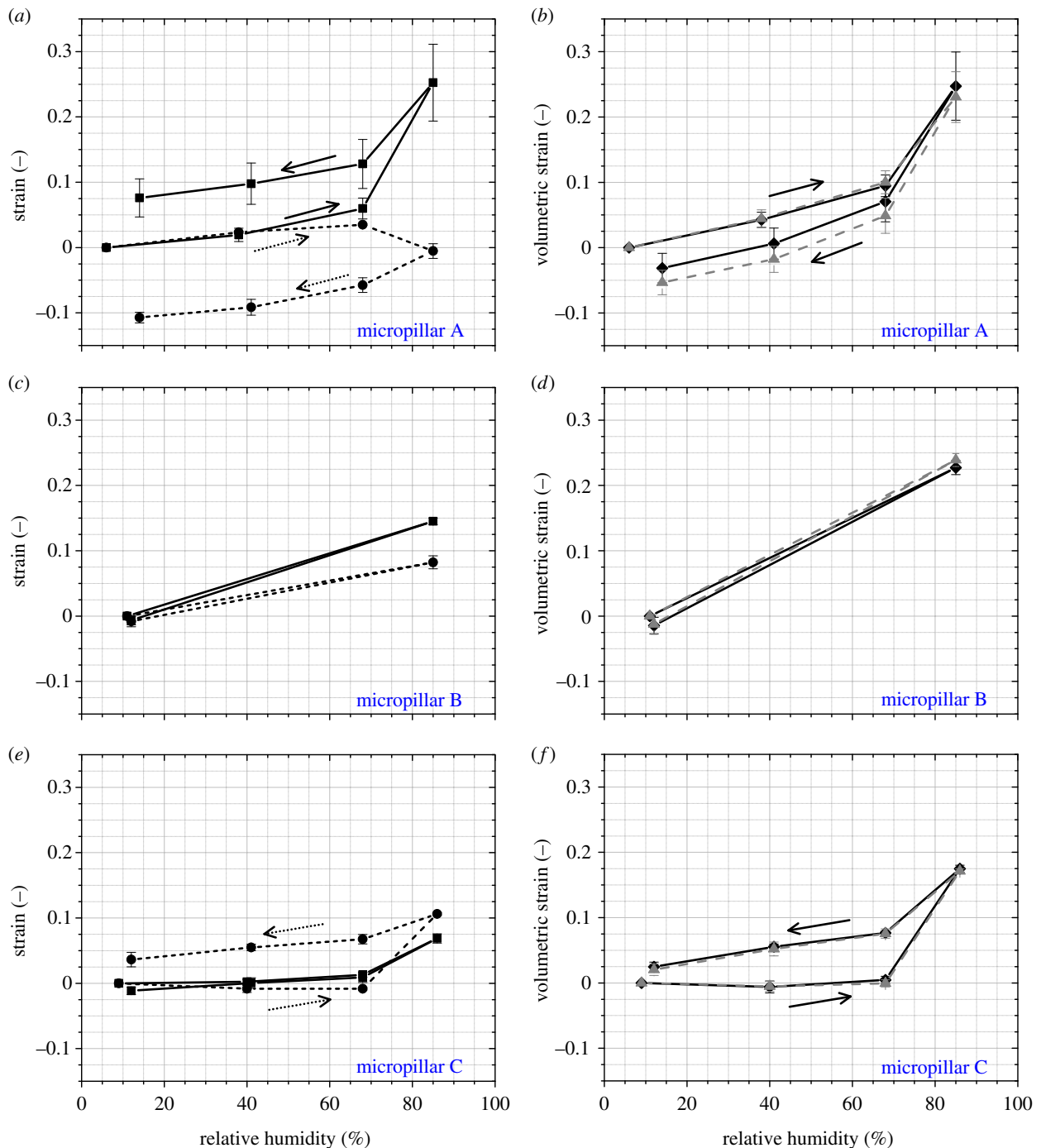


**Figure 5.** Swelling and shrinkage strains of latewood cell wall micropillars as a function of RH. (a,c,e) Mean values and the standard deviation of swelling/shrinkage strains along the directions normal (squares) and parallel (circles) to the cell wall thickness for three stacks along the height of each micropillar determined by affine registration. (b,d,f) Volumetric strains of micropillars determined by affine registration (diamonds), as the sum of normal and parallel strain components, and by voxel counting (triangles) of segmented images. (Online version in colour.)

function of MC [3]. In figure 7, we compared the transverse swelling coefficients of micropillars A, B and C with those reported in the literature at cellular tissue [7,8] and macroscopic levels for Norway spruce [28]. In this figure, the swelling coefficients of two earlywood samples (called EW1 and EW2) and two latewood samples (called LW1 and LW2) are presented. As the micropillars are very small, their MC cannot be measured. Therefore, we assumed that the MC of latewood micropillars are the same as MC of latewood sample (LW1) which can be found in [8]. This assumption is reasonable as moisture sorption is mainly related to the chemical components which are the same in sensibly similar proportion in S2 and in the whole cell [29]. Based on this assumption, the change of MC

of latewood tissue is about  $\Delta MC = 12\%$  in the RH range  $10 \rightarrow 85\%$ . The swelling coefficients are obtained simply from the relation  $\beta = \Delta \epsilon / \Delta MC$  between two RH states. We found that the volumetric strains at the cell wall level are significantly larger than those observed at cellular tissues and macroscopic wood samples composed of several growth rings. This considerable reduction in swelling/shrinkage strains at larger scales can be attributed to the unique hierarchical structure of wood cells as was first speculated by Barkas [30]. In the S2 layer, the fibril orientation is nearly parallel to the long axis of the cell. As a result, it expands transversely in proportion to the moisture change. On the other hand, the fibril orientation in the thinner S1 and inner S3 layers is more nearly

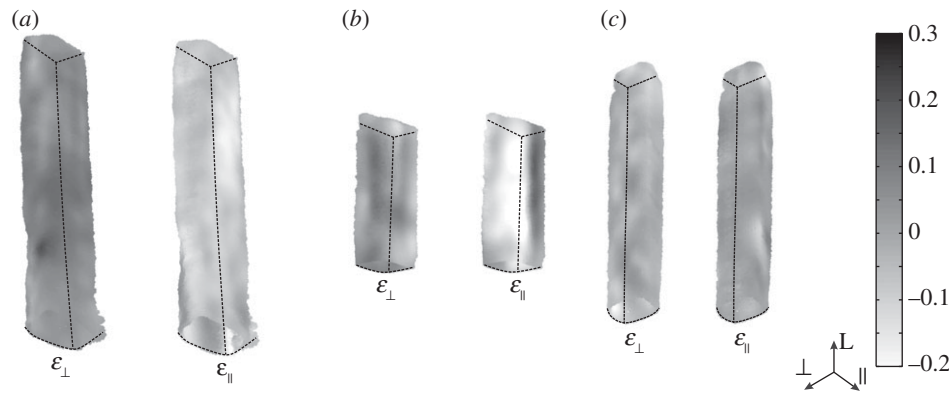


**Figure 6.** Local strain distribution of latewood cell wall micropillars for  $RH \approx 85\%$  in  $\perp$  and  $\parallel$  directions. (a) Micropillar A, (b) micropillar B and (c) micropillar C.

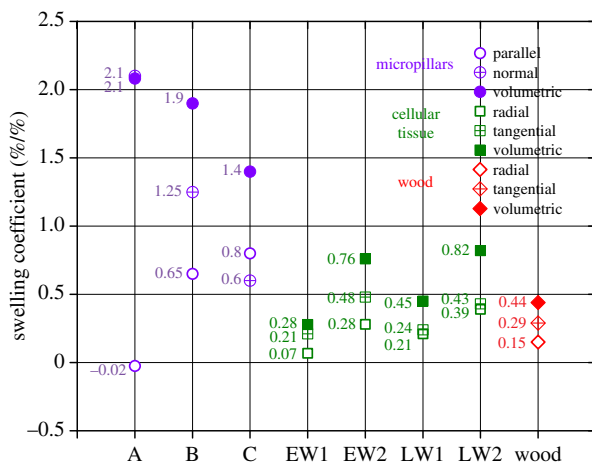


**Figure 7.** Comparing the anisotropic swelling of wood at three hierarchical levels. The MC change of micropillars A, B and C is assumed to be equal to latewood which is about 12% in the RH range  $10 \rightarrow 85\%$ . The experimental swelling coefficients of earlywood (EW1 and EW2) and latewood (LW1 and LW2) cells are taken from [8] and the data for macroscopic Norway spruce wood sample are obtained from [28]. (Online version in colour.)

perpendicular to the cell axis and tends to restrain the external and internal dimensional changes in the secondary wall because they are strong in this direction [3] and act as corsets due to the winding of the fibrils [2]. The net consequence of such hierarchical configuration is the reduced swelling deformation at higher scales (cellular tissue and growth ring) which is much less than what we observed for micropillars A and B. These two micropillars are cut out from the S2 cell wall layer. Based on these observations, we may conclude that, on removing the restraining sheath layers, the swelling capacity of the cell wall increases. The volumetric strain for swelling of micropillars A and B is about  $\varepsilon_v = 0.25$ . On the other hand, micropillar C exhibits different swelling behaviour with less volumetric swelling ( $\varepsilon_v = 0.17$ ) in comparison to micropillars A and B. In micropillar C, being bi-layer, the same deformation is hindered by the presence of the S1 layer. Therefore, it is likely that the interaction of different layers tends to reduce the total swelling capacity of the material. Based on this hypothetical explanation, the complex hierarchical structure of wood enhances the dimensional stability of wood across scales from cell wall substance to cellular tissue and to macroscopic scales. These observations are in the same direction as recent findings in our own micromechanics

investigations that show the anisotropic swelling behaviour of cellular materials is essentially due to the swelling anisotropy of the cell wall material [31,32].

Reported values in the literature for *in situ* swelling or shrinkage of latewood cell walls of softwoods obtained by microscopic observations are comparable to our measurements. The shrinkage of Norway spruce cell walls in thickness direction from wet state (approx. 80% RH) to oven dry state (approx. 103°C) is about  $\varepsilon_{\perp} = 0.28$  [33]. Ishimaru & Iida [4] measured the swelling of hinoki softwood from oven dry state (approx. 105°C) to wet state for different liquids and found that the cell walls swell to a much less extent in  $\parallel$  direction than in  $\perp$  direction. The normal swelling of latewood cell walls of hinoki softwood in liquid water is about  $\varepsilon_{\perp} = 0.21$  and volumetric swelling strain is  $\varepsilon_v = 0.28$ . Also, for an increase in RH of  $10 \rightarrow 85\%$ , the swelling strains of latewood cell walls of Douglas fir are  $\varepsilon_{\parallel} = 0.04$  and  $\varepsilon_{\perp} = 0.1$  for tangential cell walls and,  $\varepsilon_{\parallel} = 0.04$  and  $\varepsilon_{\perp} = 0.06$  for radial cell walls [5].

We observed that the swelling/shrinkage is anisotropic in the transverse plane of micropillars. For micropillars A and B, the swelling strain is larger in the normal ( $\perp$ ) than the parallel ( $\parallel$ ) direction of the cell wall thickness. This anisotropy is induced by the composite nature of the cell wall material. One explanation for transverse swelling/shrinkage anisotropy at the sub-cell wall level is given by Boutelje [11]. This model is based on the assumption of a sub-microscopically concentric lamellae pattern built up of cellulose microfibrils in the transverse plane of the S2 layer as evidenced when observing the structure of the cross section of the cell wall by atomic force microscopy [16]. Boutelje proposed that the larger part of the adsorbed water may be contained between the aforementioned concentric fibril lamellae. Thus, the adsorbed water would displace more the lamellae one from the other in  $\perp$  direction, than in  $\parallel$  direction. This description of water distribution in the cell wall is consistent with experimental observations that show the swelling and shrinkage in the transverse plane are of much greater magnitude in the direction perpendicular ( $\perp$ ) to the cell wall than parallel ( $\parallel$ ) to the cell wall as reported in literature [4,11,12] and as also presented in this work. However, the width of these lamellae is in the order of the width of a single cellulose aggregate, i.e. about 20 nm [16] which is smaller than the resolution of the imaging method used here.

The presence of microfibrils in the cell wall is also likely to induce anisotropy of swelling. As the microfibrils are approximately parallel in a helicoidal manner, the global angle or MFA could explain anisotropy [29]. The relationship

between MFA and longitudinal shrinkage is presented in the experimental study performed by Meylan [34] which shows that the longitudinal shrinkage is very low at small MFA and shows a rapid increase at  $MFA \approx 30^\circ$ . On the other hand, in the transverse plane of the cell walls, the relationship between MFA and the swelling anisotropy is rarely investigated. The role of MFA can be observed by comparing the transverse swelling and shrinkage behaviour of normal wood with compression wood which has a much higher MFA in the order of  $MFA \approx 45^\circ$ . Experiments on macroscopic samples show that the tangential swelling/shrinkage of compression wood is considerably smaller than normal wood while the longitudinal swelling is much larger in compression wood [35,36]. Dependency of the transverse shrinkage on the MFA in the range below  $MFA \approx 30^\circ$  is not notable [37]. We can estimate the influence of MFA on swelling anisotropy by incorporating simple micro-mechanical models proposed for prediction of the effective thermal expansion and moisture swelling properties of fibre-reinforced composites [38]. When MFA is close to zero, the S2 layer can be considered as a statistically transversely isotropic fibre composite with the swelling coefficients in fibre direction ( $\beta_L$ ) and transverse to the fibres ( $\beta_T$ ) given by

$$\beta_L = \beta_m \left( 1 - \frac{1}{1/K_f - 1/K_m} \left[ \frac{3(1 - 2\nu_L)\nu_L}{E_L} - \frac{1}{K_m} \right] \right) \quad (4.1)$$

and

$$\beta_T = \beta_m \left( 1 - \frac{1}{1/K_f - 1/K_m} \left[ \frac{3}{2K} - \frac{3(1 - 2\nu_L)\nu_L}{E_L} - \frac{1}{K_m} \right] \right), \quad (4.2)$$

where  $\beta_m$  is the swelling coefficient of the matrix,  $K_f$  and  $K_m$  are the bulk moduli of fibre and matrix, and  $K$ ,  $E_L$  and  $\nu_L$  are the effective bulk modulus, longitudinal elastic modulus and Poisson's ratio of the composite material, respectively. By transforming the swelling coefficients tensor with a rotation ( $\mathbf{R}$ ) equal to the MFA around the  $\perp$ -axis, we can determine  $\beta_\perp$  and  $\beta_\parallel$  from the components of the transformed swelling coefficient tensor which is written in matrix form as  $\tilde{\beta} = \mathbf{R}\beta\mathbf{R}^T$ . The preferential direction of stiff cellulose microfibrils within the S2 layer is expected to restrain swelling probably more in parallel direction than normal to the cell wall thickness. Considering that the S2 layer is composed of an almost equal quantity of stiff non-swelling crystalline cellulose ( $E_f \approx 134$  GPa) and a soft polymeric matrix ( $E_m \approx 2$  GPa), for  $MFA = 30^\circ$ , the resulting anisotropy in the transverse swelling properties of the S2 layer is approximately, according to equations (4.1) and (4.2),  $\beta_\perp/\beta_\parallel \approx 1.3$ . Therefore, considering the small MFA of S2 layer which is generally in the range  $10^\circ$ – $30^\circ$ , we may conclude that the MFA would thus be a

factor of minor importance for swelling/shrinkage anisotropy in the transverse direction. Further investigation of swelling/shrinkage behaviour of earlywood and latewood cell walls at the quasi-molecular scales should complement our understanding about the swelling behaviour of wood at the ultrastructural level.

## 5. Conclusion

In this work, high-resolution nano-tomography measurements of the swelling/shrinkage of FIB-fabricated micropillars from the thickest secondary wall of latewood cells (S2 layer) of Norway spruce exposed to varying RH conditions have been performed for the first time. Image analysis of the acquired datasets reveals that the swelling/shrinkage strains are anisotropic within the cross section of the S2 layer. It is found that the moisture-induced strains are larger in the direction normal to the cell walls than in the direction parallel to the cell walls. This investigation shows that the cell wall undergoes much higher volumetric swelling/shrinkage strains than those observed for wood at the cellular tissue level and the timber scale. The complex hierarchical structure of wood provides the material with an optimum configuration which reduces the swelling/shrinkage strains and increases its dimensional stability in humid environment. We conclude that the polymeric components configurations such as the concentric lamellae structure of cellulose microfibrils may play a crucial role in anisotropic swelling/shrinkage behaviour of the S2 layer in the transverse plane. Therefore, the swelling/shrinkage anisotropy at the cell wall level cannot be explained solely by MFA of cellulose microfibrils since their restraining effect in the range  $10^\circ$ – $30^\circ$  is not strong enough to produce large transverse anisotropy. More investigations are needed to gain further insight into the swelling/shrinkage anisotropy of the wood cell wall substance and translation of this anisotropy into higher levels of hierarchy. We believe that the proposed method can be used efficiently to accomplish this goal.

**Acknowledgement.** The contributions and support of Prof. Dr Marco Stampanoni (ETH Zurich and Paul Scherrer Institute) are greatly acknowledged. We would like to thank Gerhard Buerki (EMPA Laboratory for Mechanics and Materials and Nanostructures) for his contribution in the initial preparation of wood micropillars. The micropillars were fabricated at EMPA Laboratory for Electronics/Metrology/Reliability. We thank Alessandra Patera (EMPA Laboratory for Building Science and Technology) for assistance in the data acquisition and fruitful discussion on image processing and also Stephan Carl for technical support during experiment.

**Funding statement.** Financial support of the Swiss National Science Foundation (SNF) under grant no. 125184 is greatly acknowledged.

## References

1. Reyssat E, Mahadevan L. 2009 Hygromorphs: from pine cones to biomimetic bilayers. *J. R. Soc. Interface* **6**, 951–957. (doi:10.1098/rsif.2009.0184)
2. Derome D, Rafsanjani A, Patera A, Guyer R, Carmeliet J. 2012 Hygromorphic behaviour of cellular material: hysteretic swelling and shrinkage of wood probed by phase contrast X-ray tomography. *Philos. Mag.* **92**, 3680–3698. (doi:10.1080/14786435.2012.715248)
3. Skaar C. 1988 *Wood–water relations*. Berlin, Germany: Springer.
4. Ishimaru Y, Iida I. 2001 Transverse swelling behavior of hinoki (*Chamaecyparis obtusa*) revealed by the replica method. *J. Wood Sci.* **47**, 178–184. (doi:10.1007/BF01171219)
5. Murata K, Masuda M. 2006 Microscopic observation of transverse swelling of latewood tracheid: effect of macroscopic/mesoscopic structure. *J. Wood Sci.* **52**, 283–289. (doi:10.1007/s10086-005-0760-5)
6. Ma Q, Rudolph V. 2006 Dimensional change behavior of Caribbean pine using an environmental scanning electron microscope. *Drying Technol.* **24**, 1397–1403. (doi:10.1080/07373930600952743)
7. Derome D, Griffa M, Koebel M, Carmeliet J. 2011 Hysteretic swelling of wood at cellular scale probed by phase-contrast X-ray tomography.

- J. Struct. Biol.* **173**, 180–190. (doi:10.1016/j.jsb.2010.08.011)
8. Patera A, Derome D, Griffa M, Carmeliet J. 2013 Hysteresis in swelling and in sorption of wood tissue. *J. Struct. Biol.* **182**, 226–234. (doi:10.1016/j.jsb.2013.03.003)
  9. Badel E, Perré P. 2001 Using a digital X-ray imaging device to measure the swelling coefficients of a group of wood cells. *NDT & E Int.* **34**, 345–353. (doi:10.1016/S0963-8695(00)00072-4)
  10. Taylor A, Plank B, Standfest G, Petutschnigg A. 2013 Beech wood shrinkage observed at the microscale by a time series of X-ray computed tomographs ( $\mu$ XCT). *Holzforschung* **67**, 201–205. (doi:10.1515/hf-2012-0100)
  11. Boutelje JB. 1962 The relationship of structure to transverse anisotropy in wood with reference to shrinkage and elasticity. *Holzforschung* **16**, 33–46. (doi:10.1515/hfsg.1962.16.2.33)
  12. Murata K, Masuda M. 2001 Observation of microscopic swelling behavior of the cell wall. *J. Wood Sci.* **47**, 507–509. (doi:10.1007/BF00767907)
  13. Mellerowicz EJ, Sundberg B. 2008 Wood cell walls: biosynthesis, developmental dynamics and their implications for wood properties. *Curr. Opin. Plant Biol.* **11**, 293–300. (doi:10.1016/j.pbi.2008.03.003)
  14. Diotallevi F, Mulder B. 2007 The cellulose synthase complex: a polymerization driven supramolecular motor. *Biophys. J.* **92**, 2666–2673. (doi:10.1529/biophysj.106.099473)
  15. Dinwoodie JM. 1981 *Timber: its nature and behaviour*. New York, NY: Van Nostrand Reinhold.
  16. Fahlén J, Salmén L. 2002 On the lamellar structure of the tracheid cell wall. *Plant Biol.* **4**, 339–345. (doi:10.1055/s-2002-32341)
  17. Maloney TC, Paulapuro H. 1999 The formation of pores in the cell wall. *J. Pulp Paper Sci.* **25**, 430–436.
  18. Berthold J, Rinaudo M, Salmén L. 1996 Association of water to polar groups; estimations by an adsorption model for ligno-cellulosic materials. *Colloids Surf. A Physicochem. Eng. Aspects* **112**, 117–129. (doi:10.1016/0927-7757(95)03419-6)
  19. Orso S, Wegst U, Arzt E. 2006 The elastic modulus of spruce wood cell wall material measured by an *in situ* bending technique. *J. Mater. Sci.* **41**, 5122–5126. (doi:10.1007/s10853-006-0072-1)
  20. Adusumalli RB, Raghavan R, Ghisleni R, Zimmermann T, Michler J. 2010 Deformation and failure mechanism of secondary cell wall in Spruce late wood. *Appl. Phys. A Mater. Sci. Process.* **100**, 447–452. (doi:10.1007/s00339-010-5847-1)
  21. Zhang X, Zhao Q, Wang S, Trejo R, Lara-Curzio E, Du G. 2010 Characterizing strength and fracture of wood cell wall through uniaxial micro-compression test. *Compos. Part A Appl. Sci. Manuf.* **41**, 632–638. (doi:10.1016/j.compositesa.2010.01.010)
  22. Raghavan R, Adusumalli RB, Buerki G, Hansen S, Zimmermann T, Michler J. 2012 Deformation of the compound middle lamella in spruce latewood by micro-pillar compression of double cell walls. *J. Mater. Sci.* **47**, 6125–6130. (doi:10.1007/s10853-012-6531-y)
  23. Stampanoni M, Mokso R, Marone F, Vila-Comamala J, Gorelick S, Trtik P, Jefimovs K, David C. 2010 Phase-contrast tomography at the nanoscale using hard X-rays. *Phys. Rev. B* **81**, 140105. (doi:10.1103/PhysRevB.81.140105)
  24. Cousins WJ. 1976 Elastic modulus of lignin as related to moisture content. *Wood Sci. Technol.* **10**, 9–17. (doi:10.1007/BF00376380)
  25. Cousins WJ. 1978 Young's modulus of hemicellulose as related to moisture content. *Wood Sci. Technol.* **12**, 161–167. (doi:10.1007/BF00372862)
  26. Klein S, Staring M, Murphy K, Viergever MA, Pluim JPW. 2010 Elastix: a toolbox for intensity-based medical image registration. *IEEE Trans. Med. Imaging* **29**, 196–205. (doi:10.1109/TMI.2009.2035616)
  27. Prewitt JMS, Mendelsohn ML. 1966 The analysis of cell images. *Ann. NY Acad. Sci.* **128**, 1035–1053. (doi:10.1111/j.1749-6632.1965.tb11715.x)
  28. Rafsanjani A, Lanvermann C, Niemz P, Carmeliet J, Derome D. 2013 Multiscale analysis of free swelling of Norway spruce. *Compos. Part A Appl. Sci. Manuf.* **54**, 70–78. (doi:10.1016/j.compositesa.2013.07.005)
  29. Preston RD. 1974 *The physical biology of plant cell walls*. London, UK: Chapman and Hall.
  30. Barkas WW. 1946 Sorption, swelling and elastic constants of the cell wall material in wood. *Trans. Faraday Soc.* **42**, 137–150. (doi:10.1039/tf946420b137)
  31. Rafsanjani A, Derome D, Carmeliet J. 2013 Micromechanics investigation of hygro-elastic behavior of cellular materials with multi-layered cell walls. *Compos. Struct.* **95**, 607–611. (doi:10.1016/j.compstruct.2012.08.017)
  32. Rafsanjani A, Derome D, Guyer RA, Carmeliet J. 2013 Swelling of cellular solids: from conventional to re-entrant honeycombs. *Appl. Phys. Lett.* **102**, 211907. (doi:10.1063/1.4807844)
  33. Ermeydan MA, Cabane E, Masic A, Koetz J, Burgert I. 2012 Flavonoid insertion into cell walls improves wood properties. *ACS Appl. Mater. Interfaces* **4**, 5782–5789. (doi:10.1021/am301266g)
  34. Meylan BA. 1972 The influence of microfibril angle on the longitudinal shrinkage–moisture content relationship. *Wood Sci. Technol.* **6**, 293–301. (doi:10.1007/BF00357051)
  35. Abe K, Yamamoto H. 2006 Behavior of the cellulose microfibril in shrinking woods. *J. Wood Sci.* **52**, 15–19. (doi:10.1007/s10086-005-0715-x)
  36. Burgert I, Eder M, Gierlinger N, Fratzl P. 2007 Tensile and compressive stresses in tracheids are induced by swelling based on geometrical constraints of the wood cell. *Planta* **226**, 981–987. (doi:10.1007/s00425-007-0544-9)
  37. Yamamoto H, Sassus F, Ninomiya M, Gril F. 2001 A model of anisotropic swelling and shrinking process of wood. *Wood Sci. Technol.* **35**, 167–181. (doi:10.1007/s002260000074)
  38. Rosen BW, Hashin Z. 1970 Effective thermal expansion coefficients and specific heats of composite materials. *Int. J. Eng. Sci.* **8**, 157–173. (doi:10.1016/0020-7225(70)90066-2)